

See discussions, stats, and author profiles for this publication at: <https://www.researchgate.net/publication/271334891>

Controlling the Energy Transfer via Multi Luminescent Centers to Achieve White Light/Tunable Emissions in a Single-Phased X_2 -Type $\text{Y}_2\text{SiO}_5:\text{Eu}^{3+},\text{Bi}^{3+}$ Phosphor For Ultraviolet C...

ARTICLE *in* INORGANIC CHEMISTRY · JANUARY 2015

Impact Factor: 4.76 · DOI: 10.1021/ic502439k · Source: PubMed

CITATIONS

9

READS

33

3 AUTHORS, INCLUDING:



Mingying Peng

School of Materials Science and Engineering

139 PUBLICATIONS 3,042 CITATIONS

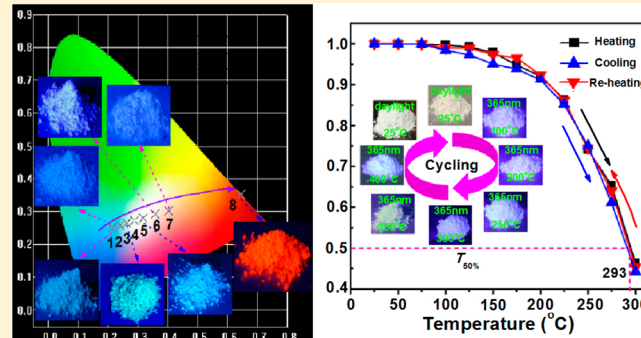
[SEE PROFILE](#)

Controlling the Energy Transfer via Multi Luminescent Centers to Achieve White Light/Tunable Emissions in a Single-Phased X2-Type $\text{Y}_2\text{SiO}_5:\text{Eu}^{3+},\text{Bi}^{3+}$ Phosphor For Ultraviolet Converted LEDs

Fengwen Kang, Yi Zhang, and Mingying Peng*

The China-Germany Research Center for Photonic Materials and Devices, The State Key Laboratory of Luminescent Materials and Devices and Guangdong Provincial Key Laboratory of Fiber Laser Materials and Applied Techniques, School of Materials Science and Engineering, South China University of Technology, Guangzhou 510641, China

ABSTRACT: So far, more than 1000 UV converted phosphors have been reported for potential application in white light-emitting diodes (WLEDs), but most of them (e.g., $\text{Y}_2\text{O}_3:\text{Eu}$, YAG:Ce or $\text{CaAlSiN}_3:\text{Eu}$) suffer from intrinsic problems such as thermal instability, color aging or re-absorption by commixed phosphors in the coating of the devices. In this case, it becomes significant to search a single-phased phosphor, which can efficiently convert UV light to white lights. Herein, we report a promising candidate of a white light emitting X2-type $\text{Y}_2\text{SiO}_5:\text{Eu}^{3+},\text{Bi}^{3+}$ phosphor, which can be excitable by UV light and address the problems mentioned above. Single Bi^{3+} -doped X2-type Y_2SiO_5 exhibits three discernible emission peaks at ~ 355 , ~ 408 , and ~ 504 nm, respectively, upon UV excitation due to three types of bismuth emission centers, and their relative intensity depends tightly on the incident excitation wavelength. In this regard, proper selection of excitation wavelength can lead to tunable emissions of $\text{Y}_2\text{SiO}_5:\text{Bi}^{3+}$ between blue and green, which is partially due to the energy transfer among the Bi centers. As a red emission center Eu^{3+} is codoped into $\text{Y}_2\text{SiO}_5:\text{Bi}^{3+}$, energy transfer has been confirmed happening from Bi^{3+} to Eu^{3+} via an electric dipole–dipole (d–d) interaction. Our experiments reveal that it is easily realizable to create the white or tunable emissions by adjusting the Eu^{3+} content and the excitation schemes. Moreover, a single-phased white light emission phosphor, X2-type $\text{Y}_{1.998}\text{SiO}_5:0.01\text{Eu}^{3+},0.01\text{Bi}^{3+}$, has been achieved with excellent resistance against thermal quenching and a QE of 78%. At 200 °C, it preserves >90% emission intensity of that at 25 °C. Consequent three time yoyo experiments of heating–cooling prove no occurrence of thermal degradation. A WLED lamp has been successfully fabricated with a CIE chromaticity coordinate (0.3702, 0.2933), color temperature 4756 K, and color rendering index of 65 by applying the phosphor onto a UV LED chip.



1. INTRODUCTION

Since Nakamura et al. reported the first phosphor-converted WLED (pc-WLED) by depositing a single-phased yellow-emitting $(\text{Y}, \text{Ga})_3(\text{Al}, \text{Ga})_5\text{O}_{12}:\text{Ce}^{3+}$ (YAG:Ce) phosphor on a blue InGaN chip (~ 460 nm),¹ pc-WLEDs have soon become commercialized and they have been coined as a new generation of light source for general illumination and display in the industry. As for the approaches to WLEDs, besides Nakamura's plan, alternatives are proposed such as (i) directly blending three primary color LED chips or (ii) combining a NUV/UV LED chip with multiple phosphors. For approach (i), it is not desirable partially because of the high manufacture costs and also because of the different chip temperatures as the chips work. In addition, this will easily give rise to poor white light luminous brightness and chromatic aberration, and it, therefore, challenges the durable white light emission. Alternatively to approach (i) and Nakamura's plan,¹ approach (ii) has been paid more attentions in these years, and it can easily realize higher color quality of lighting by simple modulating the weight ratio of RGB phosphors, such as full gamut, higher color rendering

index, lower color temperature, etc. The perception of it is more comfortable to human eyes. For this approach, it becomes essential to explore the three primary color phosphors better with strong absorption in the NUV/UV region and in the meantime not in the visible. This has motivated vigorous investigations in the area and a series of promising phosphors have been developed consequently, such as fluorides,^{2,3} silicates,⁴ phosphates,^{5–7} orthovanadates,^{8–10} borates,^{11–13} tungstates/molybdates,^{14–17} nitrides,^{18–22} aluminosilicates, or aluminates, etc.^{23–26} For the phosphors which can apply to pc-WLED via approach ii, however, there are open intrinsic problems that exist: (1) high manufacture costs because of severe preparation conditions (e.g., higher temperature and gas pressure especially for Eu^{2+} or Ce^{3+} doped nitrides^{27,28}); (2) inferior thermal and chemical stability for sulfide red phosphors; (3) absorption of longer wavelength (green or red) phosphors in visible range, which can lead to the

Received: October 7, 2014

Published: January 21, 2015

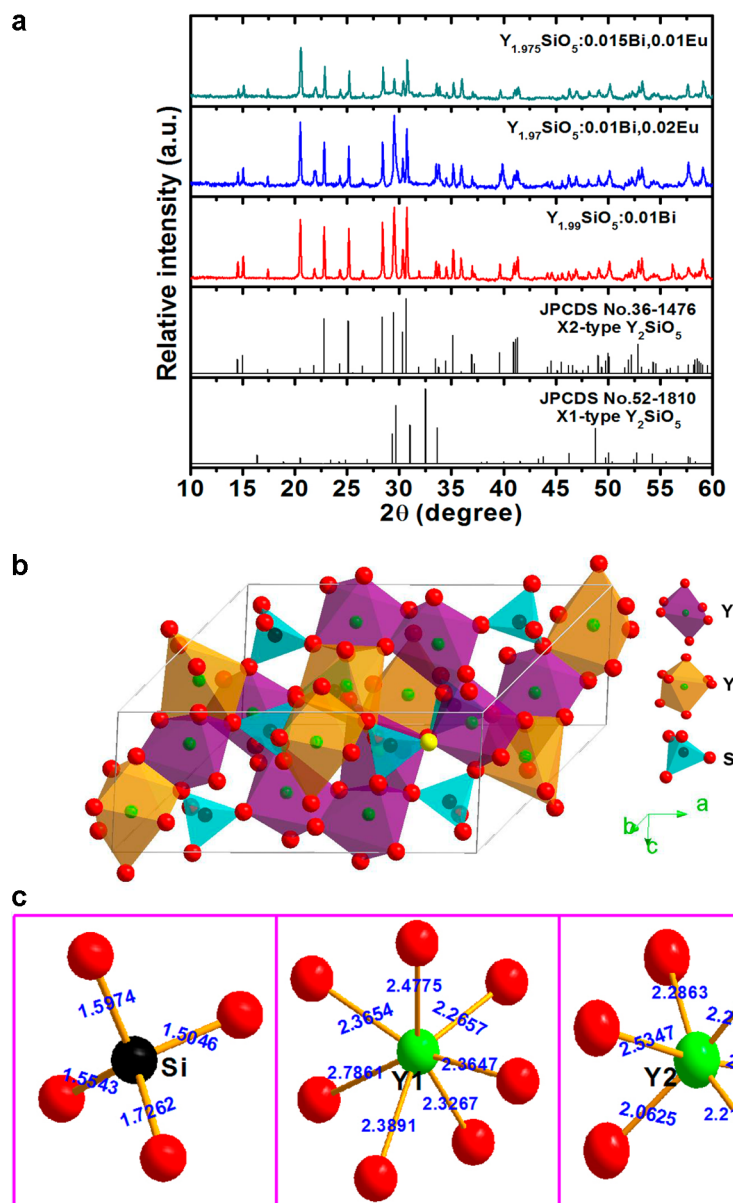


Figure 1. (a) XRD patterns of X2-type $\text{Y}_{1.99}\text{SiO}_5:0.01 \text{Bi}^{3+}$, $\text{Y}_{1.95}\text{SiO}_5:0.01 \text{Bi}^{3+},0.02\text{Eu}^{3+}$ and $\text{Y}_{1.97}\text{SiO}_5:0.015 \text{Bi}^{3+},0.01\text{Eu}^{3+}$ samples, together with the standard JCPDS cards of the monoclinic structure X1-type Y_2SiO_5 (No. 52-1810) and X2-type Y_2SiO_5 (No. 36-1476); (b) the unit cell structure of X2-type Y_2SiO_5 ; golden, pink, and blue polyhedra stand for $\text{Y}(1)\text{O}_7$, $\text{Y}(2)\text{O}_6$, and SiO_4 , respectively; yellow ball represents for an example where oxygen atom can be lost more easily, and oxygen vacancy can, therefore, be created right around the sites bismuth possibly substitutes for (c) the coordination environments of the Y^{3+} and Si^{4+} sites.

reabsorption of just-generated white lights and, therefore, the shift of CIE chromaticity coordinate due to color imbalance, and lighting distortion with lower luminous efficiency (this is especially the case for Eu^{2+} doped nitride red phosphors);²⁷ (4) different luminescence responses of multiple phosphors packed in pc-WLED to thermal impact when the temperature of LED chip increases at higher bias driving current, which can also lead to color variation of the device;^{26,29} (5) UV leakage due to inefficient absorption of the phosphors in the spectral range, which will be harmful to human healthy once exposed for longer time. In this case, if a single-phased white phosphor that could be pumped efficiently by the UV light could be developed, it might address the above problems largely. This in meanwhile can simplify the package scheme of pc-WLED.

Up to now, single-phased white light-emitting materials have been found but mainly on glasses/ceramics^{30,31} and phos-

phors.^{2,5,26,32–36} To this goal, general strategies include, which were reviewed recently by Lin et al.:³⁷ (i) blending the emissions from host and single dopant activator, for example, $\text{ZnGa}_2\text{O}_4:\text{Bi}$ or $\text{K}_2\text{EuZr}(\text{PO}_4)_3$;^{31,32} (ii) codoping multiple activators and properly managing the energy transfer between them, for example, $\text{Eu}^{2+}/\text{Mn}^{2+}$ or $\text{Ce}^{3+}/\text{Dy}^{3+}/\text{Tb}^{3+}/\text{Eu}^{3+}$;^{26–33,38} (iii) creating new type of defect which can emit white light and controlling its content by optimizing host composition and preparation conditions.^{37,39} In this work, we will follow the second strategy since it is much easier to be realized once a host compound is selected.

Yttrium orthosilicate (Y_2SiO_5) belongs to monoclinic crystal system, and it has been known as an excellent laser or scintillation host for a long time, and recently thermal barrier coating ceramics due to its high melting point (~ 2070 °C), good chemical and thermal stability.⁴⁰ For the family of

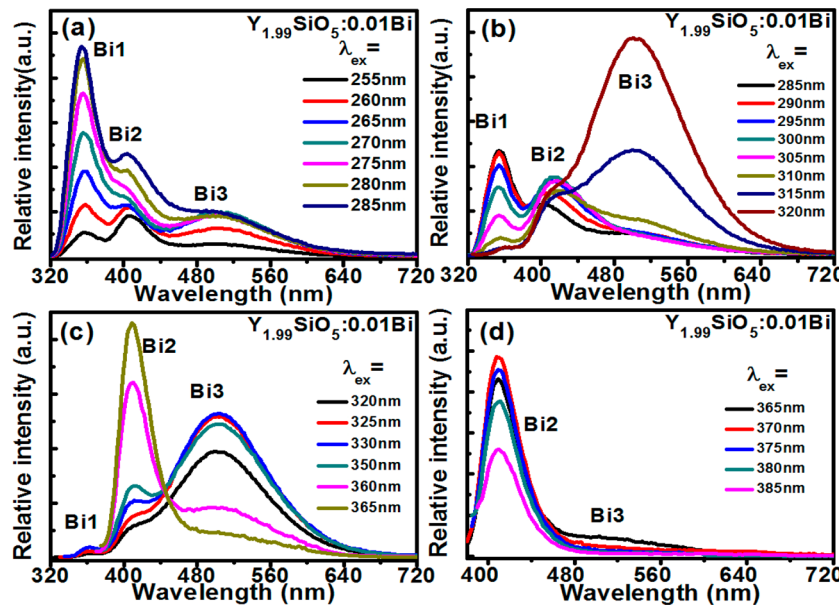


Figure 2. Emission spectra of typical sample X2-type $\text{Y}_{1.99}\text{SiO}_5:0.01\text{Bi}^{3+}$ under 255–385 nm excitations.

RE_2SiO_5 ($\text{RE} = \text{Y, La-Lu, Sc}$), two kinds of phases usually appear as the size of RE or sometimes the preparation temperature changes. For larger RE ions such as La to Tb, RE_2SiO_5 crystallizes in space group $P2_1/c$ (14) and it is denoted as X1-type RE_2SiO_5 ; while for smaller Dy to Lu and Sc ions, it turns into space group $C2/c$ (15),^{41,42} and it is known as X2-type RE_2SiO_5 . As the type of RE is set, the crystal structure will change also with temperature, for instance Y_2SiO_5 . As the preparation temperature is lowered to $\sim 1050\text{ }^\circ\text{C}$, X1-type Y_2SiO_5 is preferably formed, but it changes into X2-type Y_2SiO_5 as the temperature increases to a higher temperature ($\sim 1400\text{ }^\circ\text{C}$).⁴¹ At a temperature in between, the two phases simultaneously exist. RE ions, such as Ce^{3+} , Tb^{3+} , Eu^{3+} , Dy^{3+} , or Pr^{3+} doped either X1- or X2-type Y_2SiO_5 have been reported as well as the energy transfer between them.^{41,43–46} Yet, no white emission has been reported and realized in the single phase of Y_2SiO_5 .

In this work, we choose X2-type Y_2SiO_5 as the host rather than X1-type Y_2SiO_5 because as Lin et al. found,⁴⁷ X2-type Y_2SiO_5 is a better host for luminescent ions. As a series of work, we choose Bi^{3+} as the activator to better understand the complex behavior of bismuth in different compound. Different techniques have been utilized to reveal the luminescence dynamics of Bi^{3+} in X2-type Y_2SiO_5 , such as X-ray diffraction (XRD), quantum efficiency (QE), static and dynamic PL spectra at room and high temperature (25–300 °C). Surprisingly, we found $\text{Y}_2\text{SiO}_5:\text{Bi}^{3+}$ gives rise to three emission bands centering at ~ 355 , ~ 408 , and ~ 504 nm upon UV excitation possibly from three types of bismuth emission centers in the compound, respectively. These emissions cover almost the whole visible range from 350 to 720 nm. In view of lack of red emission in Bi^{3+} single doped X2-type Y_2SiO_5 , we intentionally introduce a secondary Eu^{3+} activator into it, and white/tunable light can, therefore, be achieved by controlling the content of Eu^{3+} or excitation schemes through managing the energy transfer from Bi^{3+} to Eu^{3+} . The mechanism has been thoroughly discussed for the energy transfer behavior. For the optimal white light-emitting sample, heating–cooling cycle experiments have been made, and three rounds of the cycle prove excellent thermal stability of the phosphor, which in turn

implies the application in pc-WLED. Finally, we demonstrate that an UV converted WLED can be made once the optimal white-emitting X2-type $\text{Y}_2\text{SiO}_5:\text{Eu}^{3+},\text{Bi}^{3+}$ phosphor is coated on an UV LED chip with an emission peak at ~ 368 nm.

2. EXPERIMENTAL SECTION

2.1. Sample Preparation. Three series of X2-type $\text{Y}_{2-x}\text{SiO}_5:x\text{Bi}^{3+}$ ($x = 0–0.03$), $\text{Y}_{1.99-x}\text{SiO}_5:0.01\text{Bi}^{3+},y\text{Eu}^{3+}$ ($y = 0.0025–0.02$), $\text{Y}_{1.99-x}\text{SiO}_5:z\text{Bi}^{3+},0.01\text{Eu}^{3+}$ ($z = 0–0.015$) phosphors were designed to study the dynamic of luminescence and unravel the energy transfer mechanism, and they were synthesized by the conventional high temperature solid-state reaction. High pure Y_2O_3 (99.99%), SiO_2 (99.99%), Eu_2O_3 (99.99%), and Bi_2O_3 (99.999%) were used as starting materials. Initially, stoichiometric reagents were weighed according to the formula above and evenly mixed for 45 min (min) in an agate mortar and then prefire in an electric furnace at 1000 °C for 3 h (h) under ambient atmosphere. After that, the samples are reground for 45 min to ensure a complete mixture, and then thoroughly sintered at 1400 °C for 3 h under ambient atmosphere. Finally, the products appear white and they were ground once again for consequent measurements.

2.2. Measurements and Characterization. The phase purity of all samples was characterized by powder XRD analysis on a Bruker D8 ADVANCE diffractometer (Germany), with using a $\text{Cu K}\alpha$ radiation ($\lambda_{\text{ex}} = 1.5418\text{ \AA}$) driven by 40 kV voltage and 40 mA current. Static and dynamic PL spectra at room and high temperature (25–300 °C) were recorded by a high-resolution PL spectrometer FLS 920 (Edinburgh Instruments) in Peltier air-cooled house in the single photon counting mode. Quantum efficiency (QE) value at room temperature was measured by an integrating sphere attached to the high-resolution PL spectrometer FLS 920. For high temperature PL spectra, sample was first loaded into a holder with a circular copper substrate, the temperature of which could be controlled by a high temperature setup (Tian Jin Orient-KOJI). The unit is removable and it can be inserted into spectrometer FLS 920 for the high temperature PL. The PL scans were performed at a step of 25 °C between 25 and 300 °C. All PL results were corrected over the lamp intensity with a silicon photodiode and the PMT spectral response. In the end, the white light phosphor, X2-type $\text{Y}_{1.998}\text{SiO}_5:0.01\text{Eu}^{3+},0.01\text{Bi}^{3+}$, was coated on a UV LED chip (peaked at 368 nm) and a WLED lamp was, thus, fabricated. The related luminous efficiency, Commission International de l'Eclairage 1931 chromaticity (CIE), CRI and CT

values were evaluated for the lamp at the current of 20 mA on a photoelectricity test system (V2.00_LED spec system).

3. RESULTS AND DISCUSSION

3.1. Crystal Structure Analysis. We have examined the phase purity of all single or codoped samples by XRD. As an example, XRD patterns of $\text{Y}_{1.99}\text{SiO}_5:\text{0.01 Bi}^{3+}$, $\text{Y}_{1.97}\text{SiO}_5:\text{0.01 Bi}^{3+},\text{0.02Eu}^{3+}$ and $\text{Y}_{1.975}\text{SiO}_5:\text{0.015 Bi}^{3+},\text{0.01Eu}^{3+}$ are listed in Figure 1a together with the standard JCPDS cards of the monoclinic structure X1-type Y_2SiO_5 (No. 52-1810) and X2-type Y_2SiO_5 (No. 36-1476). Comparison between them indicates that all diffraction peaks are well consistent with X2-type Y_2SiO_5 rather than X1-type Y_2SiO_5 . This means all the samples are pure phase of X2-type Y_2SiO_5 . Building small amounts of Bi^{3+} and Eu^{3+} ions into the host does not destroy the crystal structure of the targeted phase. Figure 1b and Figure 1c show the unit cell structure of X2-type Y_2SiO_5 and the coordination environments of the Y^{3+} and Si^{4+} sites. Clearly, there are one tetrahedral silicon site and two types of Y^{3+} sites in host which are coordinated to seven and six oxygen atoms, respectively. They are denoted as Y1 and Y2 in consequence with a lower symmetry of point group C_1 .

3.2. Photoluminescence (PL) Properties of Bi^{3+} Single-Doped X2-Type Y_2SiO_5 Sample. The bismuth single-doped X2-type Y_2SiO_5 shows different luminescence upon different excitation wavelengths. Since there is no the luminescence in blank X2-type Y_2SiO_5 sample, the luminescence should be ascribed to the $^3\text{P}_1 \rightarrow ^1\text{S}_0$ transition of Bi^{3+} ions. Figure 2a–d depict the emission spectra of X2-type $\text{Y}_{1.99}\text{SiO}_5:\text{0.01 Bi}^{3+}$ sample under 255–385 nm excitation. In the figures, one can note that as the excitation wavelength changes from 255 to 330 nm, there are always three emission peaks at ~ 355 , ~ 408 , and ~ 504 nm, respectively, while as the excitation wavelength increases to longer than 370 nm, the emission peak at ~ 504 nm is gone and only the peak at ~ 408 nm is observable. Besides peak positions, the peak intensities tightly depend on the excitation wavelength. This makes it possible to tune the sample emissions between blue and green. The CIE chromaticity coordinates based on the PL results are all listed in Table 1. Figure 3a–d can vividly reflect the color modulation by proper excitation scheme in the spectral range 250–380 nm.

To elucidate why the emission color can be tuned by selection of excitation wavelength, the excitation spectra were measured and they depend on the monitored emission wavelengths as illustrated in Figure 4a. For the emission of ~ 350 nm, the excitation spectrum comprises two peaks at ~ 295 and ~ 325 nm, and the intensity of the former is stronger than that of the latter. For the ~ 408 nm emission, three excitation peaks were observed at ~ 295 , ~ 336 , and ~ 370 nm, and the peak at ~ 370 nm is the strongest. For the emission at ~ 504 nm, the strongest excitation peak was found at ~ 326 nm along with shoulder peaks at ~ 295 and ~ 336 nm. These clearly indicate that there are three types of bismuth emission centers in the compound lying at ~ 355 , ~ 408 , and ~ 504 nm and the dominant excitations of these emissions are at ~ 295 , ~ 370 , and ~ 326 nm, respectively, because of the transition from $^1\text{S}_0$ to $^3\text{P}_1$. This is further evidenced by the difference in lifetime. For instance, the average lifetime is 582.53 ns for the emission center at 408 nm, and it is 239.01 ns for the 504 nm center (see Table 2 and 3). The emission centers at ~ 355 nm and ~ 408 nm correspond to the substitution of Bi^{3+} ions for the Y(1) and Y(2) sites, respectively. This is because of the higher covalency of the Y(2) site. As Table 4 depicts, the average covalency is

Table 1. CIE Color Coordinates (x, y) for the $\text{Y}_{1.99}\text{SiO}_5:\text{0.01 Bi}^{3+}$ Phosphor under 250–380 nm Excitations

number (no.)	λ_{ex}	CIE (x, y) values	number (no.)	λ_{ex}	CIE (x, y) values
1	250	(0.2007, 0.2064)	15	320	(0.2351, 0.3830)
2	255	(0.2097, 0.2448)	16	325	(0.2350, 0.3874)
3	260	(0.2229, 0.3056)	17	330	(0.2349, 0.3816)
4	265	(0.2295, 0.3341)	18	335	(0.2340, 0.3722)
5	270	(0.2308, 0.3314)	19	340	(0.2358, 0.3809)
6	275	(0.2291, 0.3150)	20	345	(0.2374, 0.3872)
7	280	(0.2257, 0.2874)	21	350	(0.2367, 0.3817)
8	285	(0.2185, 0.2573)	22	355	(0.2294, 0.3426)
9	290	(0.2110, 0.2283)	23	360	(0.2114, 0.2504)
10	295	(0.2053, 0.2038)	24	363	(0.2013, 0.1865)
11	300	(0.2004, 0.1826)	25	365	(0.1907, 0.1462)
12	305	(0.1994, 0.1759)	26	370	(0.1778, 0.0811)
13	310	(0.2125, 0.2433)	27	375	(0.1720, 0.0526)
14	315	(0.2302, 0.3479)	28	380	(0.1696, 0.0416)

0.1261 for Y(1) and 0.1383 for Y(2). Once Bi^{3+} resides in the site, it will experience stronger crystal field interaction and therefore lead to the longer wavelength. As for the third emission center at ~ 504 nm, we think that it should correlate to the Bi^{3+} ion which is bound to an oxygen vacancy. First principle calculations have proven that oxygen vacancy is the dominant vacancy species⁴⁸ and it prefers to form on the oxygen lattice sites (O1 to O4, for instance, we label one of such sites in yellow in Figure 1b) inside SiO_4 tetrahedra instead of the interstitial oxygen site O5 which is not bonded to silicon. This is because as the calculation shows, the formation energy of oxygen vacancy is about 10% lower on the sites O1 to O4 than O5. For the convenience in consequent discussion, we denote the centers with the emission at ~ 355 nm, ~ 408 nm and ~ 504 nm as Bi1, Bi2 and Bi3, respectively.

As excitation into the dominant absorption of Bi1 in 280–295 nm, the emission peak at ~ 355 nm dominates the emission spectrum while the peaks at ~ 408 and ~ 504 nm can be detected (see Figure 2). This together with the excitation spectra of the ~ 408 and ~ 504 nm emission in Figure 4 illustrates the energy transfer from Bi1 to Bi2 and Bi3. As the excitation moves to the dominant absorption of Bi3 in 310–350 nm, the emission peak at ~ 504 nm becomes the dominant, and nevertheless, we can still see the emissions at ~ 355 and ~ 408 nm. This is a sign of energy transfer from Bi3 to Bi1 and Bi2, and it can be verified by the excitation spectra in Figure 4. The transfer exists in X2-type $\text{Y}_{2-x}\text{SiO}_5:\text{xBi}^{3+}$ as x varies between 0.0025 and 0.03 (see Figure 5a). As x increases, the dominant Bi3 emission at 504 nm increases accordingly. So do the Bi1 and Bi2 emission. As x increases to 0.0075 (which is the critical content for Bi3), the intensity of Bi3 emission is enhanced 7 times while the enhancements are 8 and 15 times for the Bi1 and Bi2 emissions, respectively. So, the energy transfer is more

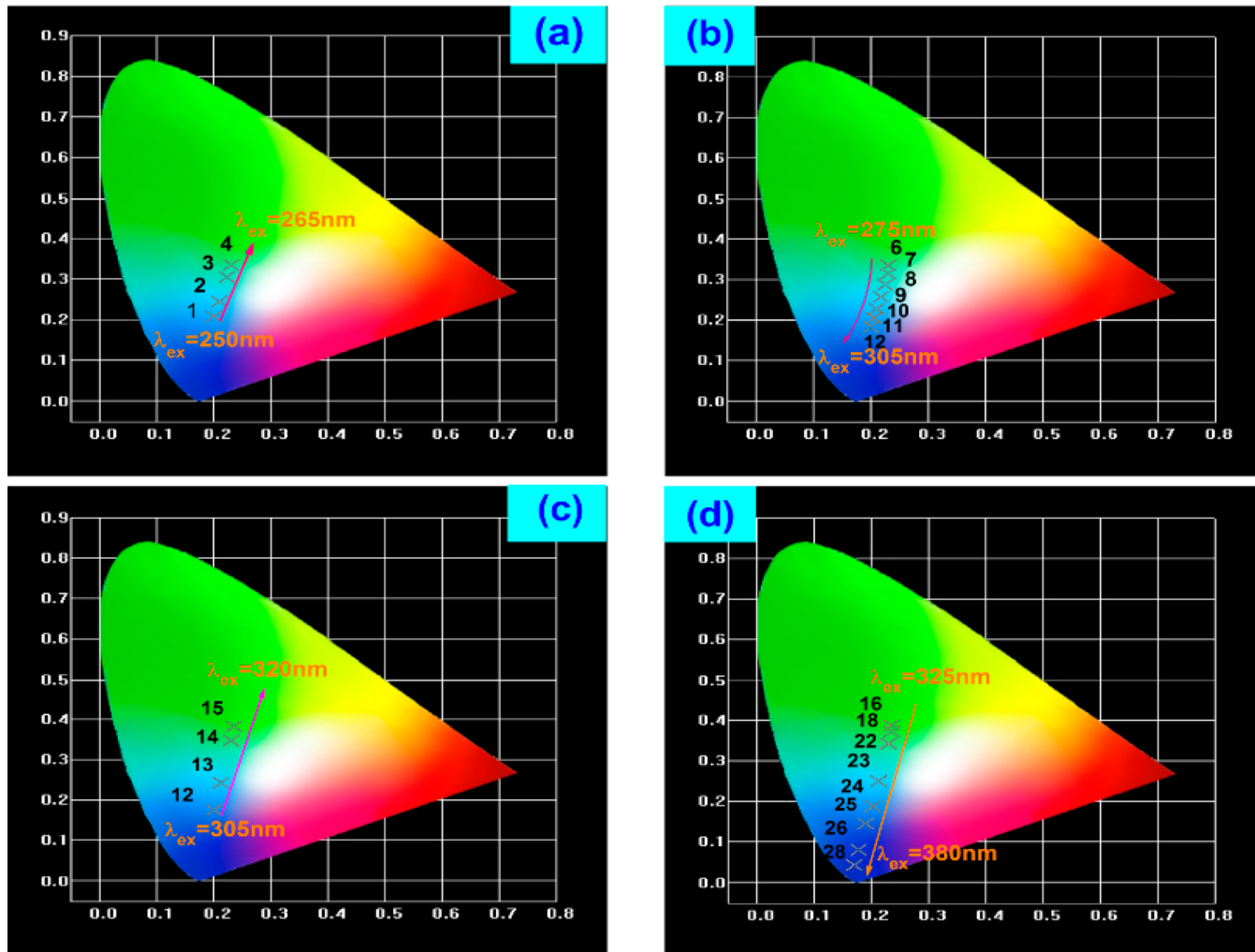


Figure 3. Typical CIE chromaticity coordinates of X2-type $\text{Y}_{1.99}\text{SiO}_5:0.01 \text{Bi}^{3+}$ sample under 250–380 nm excitations.

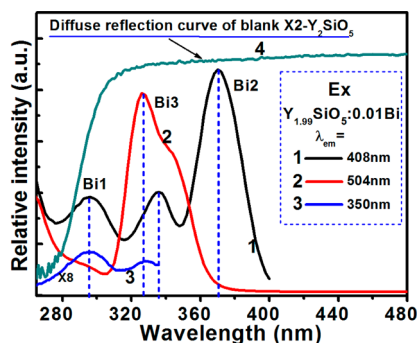


Figure 4. Excitation spectra ($\lambda_{\text{em}} = 408 \text{ nm}$ (curve 1), $\lambda_{\text{em}} = 504 \text{ nm}$ (curve 2), $\lambda_{\text{em}} = 350 \text{ nm}$ (curve 3)) of X2-type $\text{Y}_{1.99}\text{SiO}_5:0.01 \text{Bi}^{3+}$ sample and the diffused reflection spectrum of blank X2-type Y_2SiO_5 (curve 4).

efficient from Bi_3 to Bi_2 than Bi_1 . As the intensity is integrated over 350 to 700 nm, the maximum appears at 0.01 as the inset of Figure 5a shows. As the excitation changes to the absorption of $\text{Bi}(2)$ in 370–385 nm, only the emission at 408 nm is left (see Figure 2). This means no energy transfer from $\text{Bi}(2)$ to either $\text{Bi}(1)$ or $\text{Bi}(3)$. It holds for different content bismuth doped samples as Figure 5b shows. Upon excitation at 370 nm, the critical content is also 0.01 (see inset of Figure 5b).

As the excitation is into the gap where these centers share common absorptions, two or three these peaks are simultaneously observed. As excitation into the host absorption area (Figure 4 (curve 4)), that is, shorter than 280 nm, the emissions can be observed from the three centers at the same time, and the peak at 350 nm is the strongest (see Figure 2 and 4). This means the energy transfer happens from host to $\text{Bi}(1)$, $\text{Bi}(2)$ and $\text{Bi}(3)$, and the process is more efficient from the host to $\text{Bi}(1)$, since the $\text{Bi}(1)$ emission is the strongest. This is perhaps due to the better energy match of host absorption to $\text{Bi}(1)$ than the other two centers. Nevertheless, from Figure 2, we can see the energy transfer between these emission centers is not efficient since in most cases the donor and acceptor emissions can be observed in the meanwhile. This allows the color tuning of the sample emission by selecting proper excitation plan.

3.3. White Light/Tunable Emissions in X2-Type $\text{Y}_2\text{SiO}_5:\text{Eu}^{3+},\text{Bi}^{3+}$ Phosphor. As shown in Figure 2 and 3, the emissions can be tuned between blue and green for Bi^{3+} single doped sample, and it is unlike to achieve white light emission in view of insufficiency of red components. In the following, we will try to include a red emitter Eu^{3+} into the bismuth doped sample and study the possibility to generate a white emission in a single phase of Y_2SiO_5 . Figure 6a gives the excitation spectra of X2-type $\text{Y}_{1.99}\text{SiO}_5:0.01\text{Eu}^{3+}$ sample. In this

Table 2. Lifetimes ($\lambda_{\text{ex}} = 370 \text{ nm}$, $\lambda_{\text{em}} = 408 \text{ nm}$) of $\text{Y}_{1.99-y}\text{SiO}_5:0.01 \text{ Bi}^{3+},y\text{Eu}^{3+}$ ($y = 0.0025\text{--}0.02$) Samples

sample	τ_1 (ns)	A1	τ_2 (ns)	A2	γ^2	τ_{ave} (ns)
$y = 0.0000$	113.26	46.78	597.98	269.12	0.9981	582.53
$y = 0.0025$	109.76	54.09	573.18	240.98	0.9952	554.08
$y = 0.0050$	73.97	95.42	491.15	181.69	0.9969	460.57
$y = 0.0075$	89.74	121.56	489.07	149.98	0.9967	437.37
$y = 0.0100$	42.13	122.36	404.69	145.94	0.9989	375.59
$y = 0.0150$	25.25	158.27	310.48	125.46	0.9994	293.94
$y = 0.0200$	23.29	81.72	183.78	205.32	0.9976	176.07

Table 3. Lifetimes ($\lambda_{\text{ex}} = 326 \text{ nm}$, $\lambda_{\text{em}} = 504 \text{ nm}$) of $\text{Y}_{1.99-y}\text{SiO}_5:0.01 \text{ Bi}^{3+},y\text{Eu}^{3+}$ ($y = 0.0025\text{--}0.02$) Samples

sample	τ_1 (ns)	A1	τ_2 (ns)	A2	γ^2	τ_{ave} (ns)
$y = 0.0000$	64.88	37.23	246.01	244.23	0.9995	239.01
$y = 0.0025$	23.47	63.55	211.24	227.07	0.9989	205.58
$y = 0.0050$	23.34	81.85	184.10	205.26	0.9908	176.36
$y = 0.0075$	19.76	130.92	150.63	150.20	0.9956	136.82
$y = 0.0100$	19.68	145.66	123.30	140.03	0.9983	122.89
$y = 0.0150$	10.32	163.22	78.38	135.44	0.9985	118.31
$y = 0.0200$	11.28	211.56	65.58	95.26	0.9987	72.05

Table 4. Bond Length d and Chemical Bond Covalency f_c for the Y1 and Y2 Sites in X2-Type Y_2SiO_5

YO ₇			YO ₆		
bond	d (Å)	f_c	bond	d (Å)	f_c
Y1–O(1)	2.4775	0.1229	Y2–O(1)	2.2167	0.1419
Y1–O(2)	2.3891	0.1275	Y2–O(2)	2.3174	0.1357
Y1–O(3)	2.3647	0.1288	Y2–O(3)	2.2841	0.1377
Y1–O(4)	2.3267	0.1309	Y2–O(4)	2.5347	0.1241
Y1–O(5)	2.2657	0.1344	Y2–O(5)	2.2863	0.1376
Y1–O(6)	2.7861	0.1093	Y2–O(6)	2.0625	0.1525
Y1–O(7)	2.3654	0.1287			
average	2.4250	0.1261	average	2.2836	0.1383

figure, the excitation spectra monitored at 611 (curve 1) and 592 nm (curve 2) show several sharp lines consisting of 296, 322, 362, 381, 394, 415, 466, 527, and 533 nm. These lines can be assigned to the characteristic excitation peaks of Eu³⁺ ions, corresponding to the intraconfigurational transitions of $^7\text{F}_0 \rightarrow ^5\text{F}_4$, $^7\text{F}_0 \rightarrow ^5\text{H}_6$, $^7\text{F}_0 \rightarrow ^5\text{D}_4$, $^7\text{F}_0 \rightarrow ^5\text{G}_4$, $^7\text{F}_0 \rightarrow ^5\text{L}_6$, $^7\text{F}_0 \rightarrow ^5\text{D}_3$, $^7\text{F}_0 \rightarrow ^5\text{D}_2$, $^7\text{F}_0 \rightarrow ^5\text{D}_1$, and $^7\text{F}_1 \rightarrow ^5\text{D}_1$, respectively.^{14,15,44} The emission spectra of the X2-type $\text{Y}_{1.99}\text{SiO}_5:0.01\text{Eu}^{3+}$ sample excited by 270 (curve 1) and 394 nm (curve 2) are shown in Figure 6b, in which one can observe an weak emission due to the $^5\text{D}_1 \rightarrow ^7\text{F}_2$ transition and the typical Eu³⁺ emission lines of $^5\text{D}_0 \rightarrow ^7\text{F}_J$ ($J = 0, 1, 2, 3, 4$) transitions within 560–720 nm range. Among these emission lines, the dominated three peaks locate at 592, 611, and 704 nm. This is due to low C_1 symmetry of Eu³⁺ ions which are substituted for Y(1) and Y(2) sites in view of size and charge matches. These Eu³⁺ emissions in X2-type Y_2SiO_5 , together with Bi³⁺ emissions, will make the white light generation possible. We therefore made the Eu³⁺ and Bi³⁺ codoped samples. Inspecting into the excitation spectrum of $\lambda_{\text{em}} = 611 \text{ nm}$ in X2-type $\text{Y}_{1.98}\text{SiO}_5:0.01 \text{ Bi}^{3+}, 0.01\text{Eu}^{3+}$ (Figure 7a (curve 1)), it is noted that the sample not only exhibits the sharp lines of Eu³⁺ but also the excitation peaks at ~ 295 , ~ 326 , and ~ 370 nm from Bi1, Bi3, and Bi2, respectively. This is the straight evidence for the energy transfer from Bi³⁺ to Eu³⁺. The peak at ~ 326 nm dominates over the other peaks, implying a more efficient energy transfer from Bi³⁺ to Eu³⁺. The energy transfer can be further confirmed by the emission spectra upon

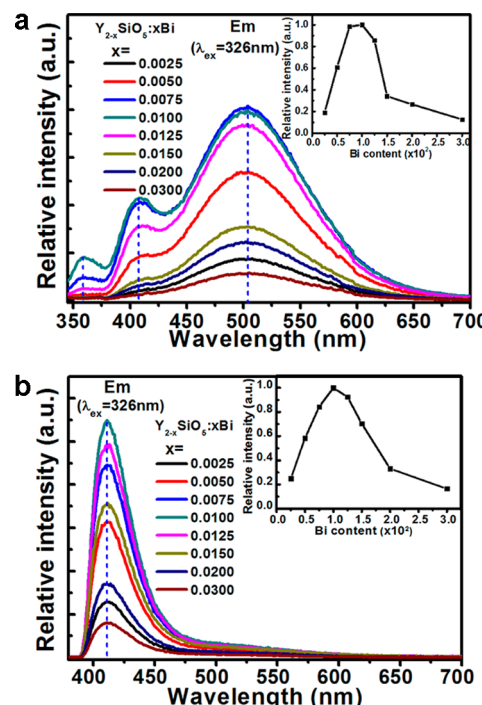


Figure 5. Emission spectra of X2-type $\text{Y}_{2-x}\text{SiO}_5:x\text{Bi}^{3+}$ ($x = 0\text{--}0.03$) under 326 (a) and 370 nm (b) excitation; the inset shows the dependence of Bi³⁺ content on the respective integral emission intensity.

excitation into the absorptions of Bi2 or Bi3 (see Figure 7b). In these spectra, the Eu³⁺ emission can be always observed for excitation either at 326, 360, or 370 nm. Additionally, as for the excitation into Bi3 absorption, for example, at 326 nm, both the Bi2 and Bi3 emissions were found. This implies the existence of Eu³⁺ does not block the energy transfer from Bi3 to Bi2. We also found in codoped samples that the energy transfer is unidirectional from Bi³⁺ to Eu³⁺, and there is no sign for the backward transfer from Eu³⁺ to Bi³⁺. This can be proved by the excitation curves of the emissions at 408 and 504 nm listed in Figure 7a.

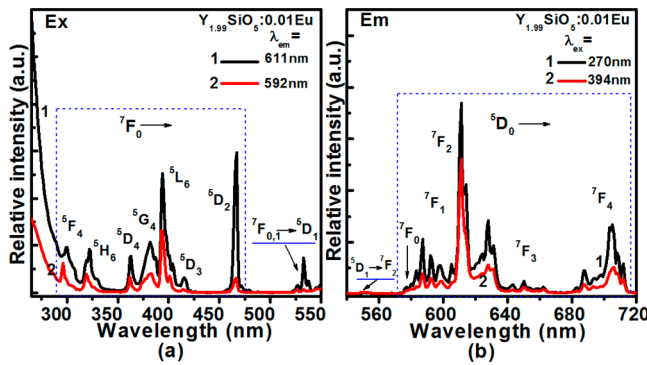


Figure 6. Excitation ($\lambda_{\text{em}} = 611 \text{ nm}$ (curve 1), $\lambda_{\text{em}} = 592 \text{ nm}$ (curve 2)) (a) and emission spectra ($\lambda_{\text{ex}} = 270 \text{ nm}$ (curve 1), $\lambda_{\text{ex}} = 394 \text{ nm}$ (curve 2)) (b) of X2-type $\text{Y}_{1.99}\text{SiO}_5:0.01\text{Eu}^{3+}$ sample.

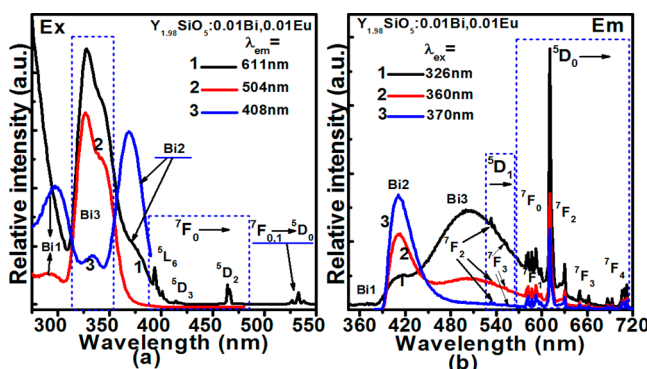


Figure 7. Excitation spectra ($\lambda_{\text{em}} = 611 \text{ nm}$ (curve 1), $\lambda_{\text{em}} = 504 \text{ nm}$ (curve 2), $\lambda_{\text{em}} = 408 \text{ nm}$ (curve 3)) (a) and emission spectra ($\lambda_{\text{ex}} = 326 \text{ nm}$ (curve 1), $\lambda_{\text{ex}} = 360 \text{ nm}$ (curve 2), $\lambda_{\text{ex}} = 370 \text{ nm}$ (curve 3)) (b) of X2-type $\text{Y}_{1.98}\text{SiO}_5:0.01\text{Bi}^{3+}, 0.01\text{Eu}^{3+}$ sample.

The energy transfer from Bi^{3+} to Eu^{3+} depends on the concentration of Eu^{3+} . Figure 8 depicts the emission spectra of $\text{Y}_{1.99-y}\text{SiO}_5:0.01\text{Bi}^{3+}, y\text{Eu}^{3+}$ ($y = 0.0025\text{--}0.02$) under 326 (a) and 370 nm (b) excitation, which corresponds to the absorptions of $\text{Bi}3$ and $\text{Bi}2$, respectively. With increasing Eu^{3+} content, the emissions at $\sim 408 \text{ nm}$ ($\text{Bi}2$ center) and $\sim 504 \text{ nm}$ ($\text{Bi}3$ center) decrease while Eu^{3+} emission increases monotonically no matter which excitation scheme it is. No quenching of Eu^{3+} emission occurs as y increases to 0.02. For excitation scheme with 370 nm, green emission can not be produced. A proper excitation wavelength has to be reconsidered and it should lead to the blue and green emissions at the same time. Figure 2 shows the 360 nm excitation is possible. So, we measured the emission spectra of codoped samples $\text{Y}_{1.99-y}\text{SiO}_5:0.01\text{Bi}^{3+}, y\text{Eu}^{3+}$ upon this excitation, as shown in Figure 8(c). Both blue and green emissions can be lead along with Eu^{3+} emission. As Eu^{3+} content increases, bismuth blue and green emissions decrease a little bit while Eu^{3+} emission continuously increases. Accordingly, the sample emission color changes from blue ($0.2114, 0.2504$) to white ($0.3172, 0.2811$) and then to a light pink ($0.4014, 0.3013$). The corresponding tunable CIE chromaticity coordinates are shown in Figure 8(d). The CIE value ($0.6461, 0.3536$) of $\text{Y}_{1.99}\text{SiO}_5:0.01\text{Eu}^{3+}$ sample upon 270 nm excitation (point 8) is also given in the figure for reference, in which a bright red is observable. The related tunable colors are visibly demonstrated by the digital photographs of the codoped samples exposed to a 365 nm lamp. One can clearly see that the Eu^{3+} content corresponding

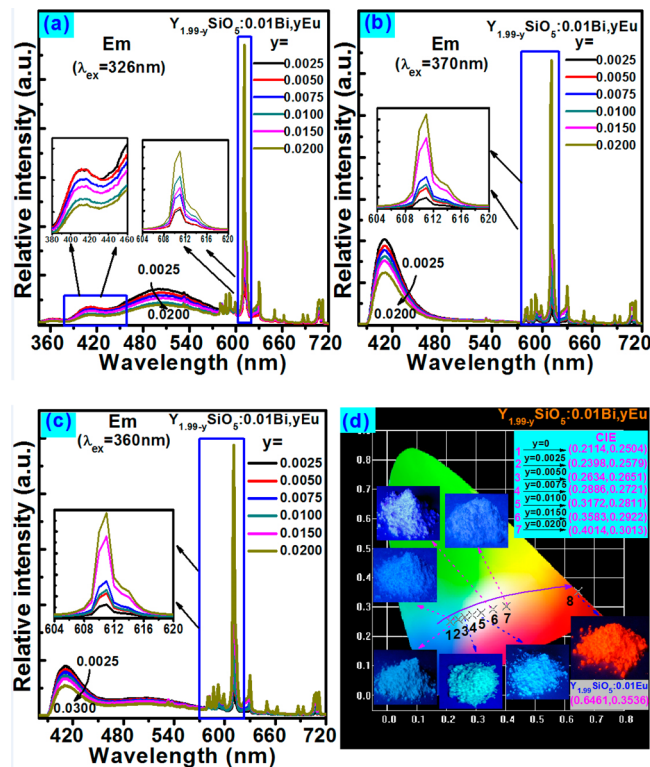


Figure 8. Emission spectra ($\lambda_{\text{ex}} = 326$ (a), $\lambda_{\text{ex}} = 370$ (b), $\lambda_{\text{ex}} = 360 \text{ nm}$ (c)) of X2-type $\text{Y}_{1.99-y}\text{SiO}_5:0.01\text{Bi}^{3+}, y\text{Eu}^{3+}$ ($y = 0.0025\text{--}0.02$) sample; (d) the CIE chromaticity coordinates of X2-type $\text{Y}_{1.99-y}\text{SiO}_5:0.01\text{Bi}^{3+}, y\text{Eu}^{3+}$ ($y = 0.0025\text{--}0.02$) sample and the sample photos (inset) under 360 nm excitation.

to the white emission is located within a range of 0.005–0.015. These results suggest it is possible to control the energy transfer from Bi^{3+} to Eu^{3+} , and therefore the emission color by Eu^{3+} content.

Similar to $\text{Y}_2\text{SiO}_5:\text{Bi}^{3+}$ (see Figure 2), for $\text{Y}_{1.98}\text{SiO}_5:0.01\text{Bi}^{3+}, 0.01\text{Eu}^{3+}$, changing the excitation wavelength from 250 to 380 nm does not change the emission positions, but it can modulate the relative intensity of Bi^{3+} and Eu^{3+} emissions, as shown in Figure 9. The tunable emissions between red, yellow blue and green can be achieved by blending the Bi^{3+} and Eu^{3+} emissions upon different excitation wavelengths. The CIE

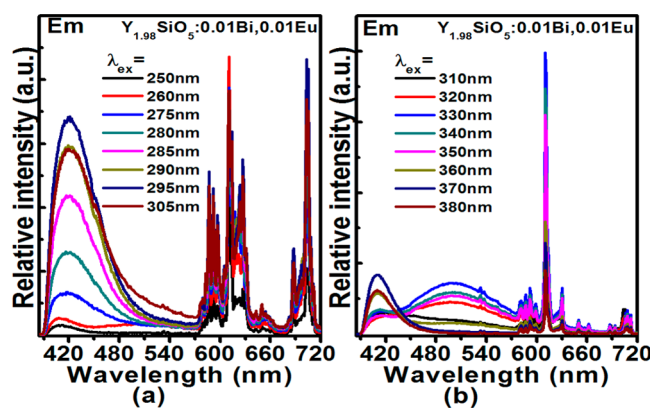


Figure 9. Emission spectra of X2-type $\text{Y}_{1.98}\text{SiO}_5:0.01\text{Bi}^{3+}, 0.01\text{Eu}^{3+}$ sample under 250–380 nm excitations.

values are included in Table 5 and some exemplary results and photos are illustrated in Figure 10.

Table 5. CIE Color Coordinates (x, y) for the $\text{Y}_{1.98}\text{SiO}_5:0.01\text{Bi}^{3+},0.01\text{Eu}^{3+}$ Phosphor under 250–370 nm Excitations

number (no.)	λ_{ex}	CIE (x, y)	number (no.)	λ_{ex}	CIE (x, y)
1	250	(0.5540, 0.3265)	17	320	(0.3168, 0.3344)
2	255	(0.5352, 0.3268)	18	322	(0.3168, 0.3465)
3	260	(0.5146, 0.3399)	19	325	(0.3168, 0.3543)
4	265	(0.5064, 0.3497)	20	327	(0.3176, 0.3555)
5	270	(0.5072, 0.3447)	21	330	(0.3182, 0.3639)
6	275	(0.4934, 0.3197)	22	332	(0.3191, 0.3518)
7	280	(0.4441, 0.2706)	23	335	(0.3189, 0.3481)
8	285	(0.3832, 0.2194)	24	337	(0.3190, 0.3485)
9	290	(0.3406, 0.1855)	25	340	(0.2189, 0.3488)
10	295	(0.3174, 0.1666)	26	345	(0.3200, 0.3541)
11	300	(0.3071, 0.1592)	27	355	(0.3187, 0.3189)
12	305	(0.3033, 0.1613)	28	360	(0.3172, 0.2881)
13	310	(0.3050, 0.1889)	29	362	(0.3113, 0.2540)
14	312	(0.3093, 0.2157)	30	365	(0.3027, 0.1886)
15	315	(0.3131, 0.2687)	31	367	(0.2956, 0.1487)
16	317	(0.3154, 0.3024)	32	370	(0.2950, 0.1333)

The energy transfer from Bi^{3+} to Eu^{3+} also depends on the concentration of Bi^{3+} . As the Eu^{3+} content is fixed as 0.01, $\text{Y}_{1.99-y}\text{SiO}_5:z\text{Bi}^{3+},0.01\text{Eu}^{3+}$ ($z = 0.0025\text{--}0.015$) phosphors were made and the PL spectra were also measured upon 326 (a) and 370 nm (b) excitation and shown in Figure 11. The Eu^{3+} emission intensity monotonically increases as the Bi^{3+} content increases. As for the Bi^{3+} emission, the emission intensity at 408 or 504 nm also initially increases and then decreases because of the concentration quenching effect. The variation of the emission intensity upon 370 nm excitation is similar to the 326 nm excitation.

3.4. Energy Transfer Mechanism from Bi^{3+} to Eu^{3+} . On the basis of the PL features presented in Figure 2, Figures 4, 5, 8, and 9, the energy transfer scheme from Bi^{3+} to Eu^{3+} is proposed as Figure 12. By exciting into Bi^{3+} absorption (path 1), for instance, at 326 nm, the typical Bi^{3+} emission appears at 504 nm (path 2) in the Bi/Eu codoped sample, at the same time, due to the energy transfer from Bi^{3+} to Bi^{3+} (path 3), the Bi^{3+} emission at 408 nm shows up (path 4). Besides the Bi^{3+} and Bi^{3+} emissions, the energy transfer happens from Bi^{3+} to Eu^{3+} (path 5) and it leads to the Eu^{3+} emissions along path 6. As the excitation wavelengths change in 312–320 nm or 330–365 nm, paths 1–6 can coexist in $\text{Y}_{1.98}\text{SiO}_5:0.01\text{Bi}^{3+},0.01\text{Eu}^{3+}$, and it leads to the white light emission (see Figure 10). Similarly, for a specific excitation scheme, for instance at 360 nm, the white emission can be achieved as Eu content changes between 0.005 and 0.015 in $\text{Y}_{1.99-y}\text{SiO}_5:0.01\text{Bi}^{3+},y\text{Eu}^{3+}$ (see Figure 8). As

exciting into Bi^{3+} absorption (path 7), for example, at 370 nm, the Bi^{3+} emission is led along with the Eu^{3+} emission due to the energy transfer from Bi^{3+} to Eu^{3+} (path 8). Tunable emissions can be achieved by selection of the excitation plans and the Bi/Eu content ratio while following paths 1–8.

For the sake of better understanding the energy transfer mechanism from Bi^{3+} to Eu^{3+} , the decay curves of X2-type $\text{Y}_{1.99-y}\text{SiO}_5:0.01\text{Bi}^{3+},y\text{Eu}^{3+}$ ($y = 0.0025\text{--}0.02$) samples were measured (see Figure 13a, b). The excitation and monitored emission wavelengths are marked in the figure. All decay curves were found following the double exponential decay equation as follows:^{5,8,49–51}

$$I(t) = A_1 \exp(-t/\tau_1) + A_2 \exp(-t/\tau_2) \quad (1)$$

where τ_1 and τ_2 are short- and long-decay components and A_1 and A_2 are the constants, respectively. The average lifetimes (τ_{ave}) are evaluated by the equation:^{5,51}

$$\tau = (A_1\tau_1^2 + A_2\tau_2^2)/(A_1\tau_1 + A_2\tau_2) \quad (2)$$

As Eu^{3+} increases from 0 to 0.0025, 0.005, 0.0075, 0.01, 0.015, and 0.02, the average lifetime τ_{ave} of the Bi^{3+} emission at 504 nm upon the excitation of 326 nm decreases from 239.01 to 205.58, 176.36, 136.82, 122.89, 118.31, and 72.05 ns. Similarly, τ_{ave} of the Bi^{3+} emission at 408 nm upon the excitation of 370 nm also decreases all the way from 582.53, to 554.08, 460.57, 437.37, 375.59, 293.94, and 176.07 ns, respectively (see Figure 13a, b). All values are listed in Tables 2 and 3, together with the goodness-of-fit γ^2 values. γ^2 is better than 99% for all the fittings. The visual lifetime reduction is an evidence for energy transfer from Bi^{3+} to Eu^{3+} . Similar phenomenon of double exponential decay for energy transfer from one ion (or host) to another ion was observed in previous reports.^{8,51,52}

With the above lifetimes, the energy transfer efficiency (η_T) from Bi^{3+} to Eu^{3+} can also be evaluated by the following expression:^{5,6,24,34,35}

$$\eta_T = 1 - \tau_s/\tau_{s0} \quad (3)$$

where τ_{s0} and τ_s are the lifetime of Bi^{3+} in the absence and presence of Eu^{3+} , respectively. Using this equation, η_{iT} from Bi^{3+} to Eu^{3+} is calculated to be 13.99%, 26.21%, 42.76%, 48.58%, 50.50%, and 69.85%, while that from Bi^{3+} to Eu^{3+} is 4.88%, 20.94%, 24.92%, 35.53%, 49.54%, and 69.78% for the Eu^{3+} content $y = 0.0025, 0.005, 0.0075, 0.01, 0.015$, and 0.02, respectively. These values are plotted as Figure 13c and d. Clearly, the energy transfer efficiency η_T increases with the Eu^{3+} content in both excitation schemes. The incomplete energy transfer allows the generation of white light or tunable emission possible.

The Dexter's theory on energy transfer was used to elucidate the possible mechanism on the energy transfer from Bi^{3+} to Eu^{3+} . If it was a multipolar-multipolar interaction process, the equation:^{5,6}

$$\frac{\eta_0}{\eta} \propto C^{n/3} \quad (4)$$

where η_0 and η are the luminescence quantum efficiencies of Bi^{3+} in the absence and presence of Eu^{3+} , respectively, C is the Eu^{3+} content, $n = 6, 8$, and 10, which corresponds to dipole-dipole (d-d), dipole-quadrupole (d-q), and quadrupole-quadrupole (q-q), respectively. Normally, the η_0/η ratio can be estimated approximately by the related luminescence intensity (I_0/I). In this case, I_0/I versus $C^{n/3}$ plots are depicted in Figure

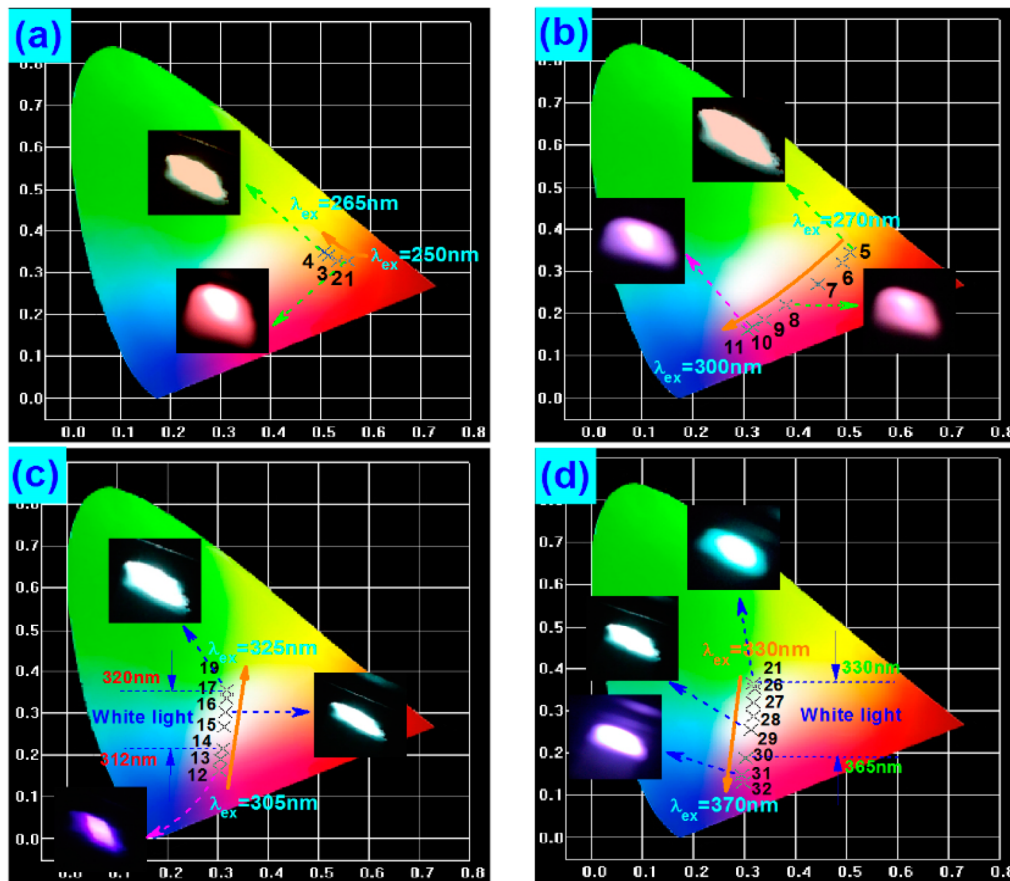


Figure 10. Typical CIE color coordinates of X2-type $\text{Y}_{1.98}\text{SiO}_5:0.01 \text{Bi}^{3+},0.01 \text{Bi}^{3+}$ sample and the sample photos under different excitations.

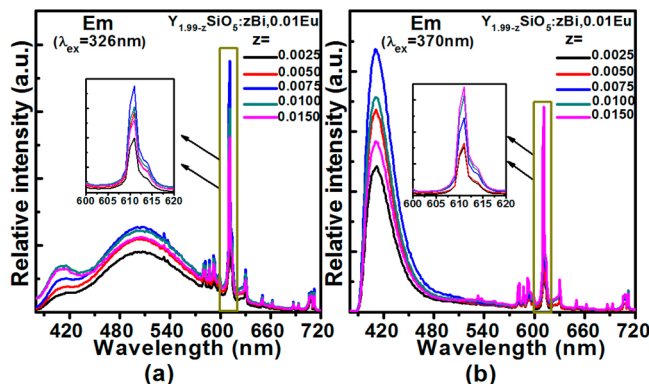


Figure 11. Emission spectra of X2-type $\text{Y}_{1.99-z}\text{SiO}_5:z\text{Bi}^{3+},0.01\text{Eu}^{3+}$ ($z = 0\text{--}0.015$) samples under 326 (a) and 370 nm (b) excitations.

14, and best fitting was found 99.75% only when $n = 6$. It implies, therefore, that the d-d interaction dominates the energy transfer from Bi^{3+} to Eu^{3+} .

3.5. Thermal Quenching Properties of White Light-Emitting X2-Type $\text{Y}_2\text{SiO}_5:\text{Eu}^{3+},\text{Bi}^{3+}$. As driving current increases, the chip temperature of LED increases accordingly. For high power LED chip, a LED chip can be heated up to more than 200 °C.^{53,54} So, for practical application of a phosphor in the area, it is necessary to evaluate the thermal quenching particularly at the temperature higher than room temperature. Therefore, the PL for the white light-emitting X2-type $\text{Y}_{1.98}\text{SiO}_5:0.01 \text{Bi}^{3+},0.01\text{Eu}^{3+}$ phosphor is measured at higher temperatures upon the excitation scheme $\lambda_{\text{ex}} = 360 \text{ nm}$,

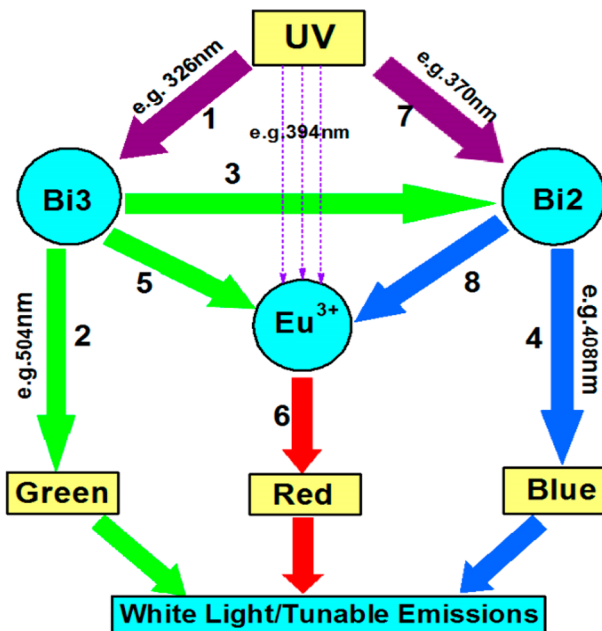


Figure 12. Energy transfer scheme for generation of white light/tunable emissions upon UV excitations. Paths 1–8 show the energy flow from light source/donor ions to activator ions.

and the results are shown in Figure 15a. It is obvious that increasing the temperature from 25 to 300 °C leads to the decrease of the emission intensity while it does not change the emission positions. Figure 15b (curve 1) plots the dependence

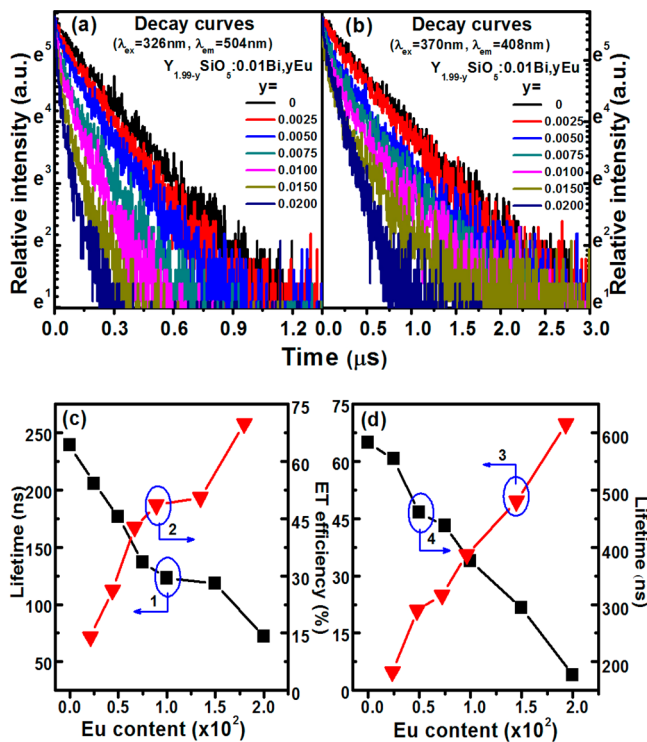


Figure 13. Decay curves ($\lambda_{\text{ex}} = 326 \text{ nm}$, $\lambda_{\text{em}} = 504 \text{ nm}$ (a); $\lambda_{\text{ex}} = 370 \text{ nm}$, $\lambda_{\text{em}} = 408 \text{ nm}$ (b)) of X2-type $\text{Y}_{1.99-y}\text{SiO}_5:0.01\text{Bi}^{3+},y\text{Eu}^{3+}$ ($y = 0.0025\text{--}0.02$); (c-d) the dependence of the fitted Bi^{3+} (I) (curve 1) and Bi^{3+} (II) (curve 4) lifetimes and the energy transfer efficiencies (η_T) (curve 2 and curve 3) on Eu^{3+} concentration.

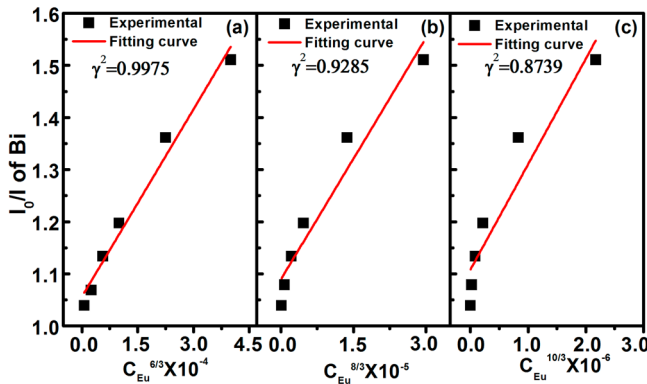


Figure 14. Dependence of I_0/I on $C_{\text{Eu}}^{(n/3)}$ in X2-type $\text{Y}_{1.99-y}\text{SiO}_5:0.01\text{Bi}^{3+},y\text{Eu}^{3+}$ ($y = 0.0025\text{--}0.02$). Correlation efficiencies are 99.75%, 92.85%, and 87.39% for the fittings to eq 4 in panels a, b, and c, respectively.

of the integrated PL intensity on the temperature. It shows that the thermal quenching temperature $T_{50\%}$ defined as the temperature at which the emission intensity decreases to 50% of $T = 25^\circ\text{C}$ is 293°C . At 200°C , the luminescence intensity remains $\sim 92\%$ of $T = 25^\circ\text{C}$. What is more, three rounds of yoyo experiments on cooling and heating cycles prove that the integrated PL intensity can be restored basically to its initial state, as depicted in Figure 15b (curve 2 and curve 3). Figure 15c records the photos of the phosphor under daylight and UV ($\sim 365 \text{ nm}$) lights at different temperatures. As temperature increases, bright white colors of the phosphor can still be observed, even though the temperature is up to 450°C .

The activation energy (ΔE_a) for the thermal quenching of luminescence was evaluated by the Arrhenian equation:^{54,55}

$$I(T) = I_0 \left[1 + c \exp\left(-\frac{\Delta E_a}{kT}\right) \right]^{-1} \quad (5)$$

where I_0 is the initial emission intensity, T is the temperature in Kelvin, $I(T)$ is the integral emission intensity at temperature T , c is a constant parameter, and k is the Boltzmann constant ($8.629 \times 10^{-5} \text{ eV}\cdot\text{K}^{-1}$). Figure 15d plots the relationship of $\ln[(I_0/I(T)) - 1]$ versus $1/kT$ for the single-phased white light-emitting X2-type $\text{Y}_{1.98}\text{SiO}_5:0.01\text{Bi}^{3+},0.01\text{Eu}^{3+}$ phosphor. Fitting to eq 5 produces ΔE_a as 0.398 eV . The activation energy is higher than (or comparable to) some of popular phosphors, such as silicates,³ nitrides,^{56,57} aluminates,⁵⁵ etc. For the probability of a nonradiative per unit time (v), it can be expressed as⁵⁵

$$v = s \exp\left(-\frac{\Delta E}{kT}\right) \quad (6)$$

where s is the frequency factor (s^{-1}). The higher ΔE_a means lower v . These results indicate that the phosphor of X2-type $\text{Y}_{1.98}\text{SiO}_5:0.01\text{Bi}^{3+},0.01\text{Eu}^{3+}$ has the better resistance to thermal quenching and degradation.

3.6. WLEDs Device Fabrication. Quantum efficiency of the white light-emitting X2-type $\text{Y}_{1.98}\text{SiO}_5:0.01\text{Bi}^{3+},0.01\text{Eu}^{3+}$ was also measured, and it is 78% upon 360 nm excitation. The result and the outstanding thermal stability of luminescence encourage us to fabricate a LEDs lamp with the phosphor. We coated the phosphor onto a UV LED chip with an emission distributed between 350 and 390 nm . Figure 16 shows the electroluminescence (EL) spectrum of the lamp at a bias current 20 mA . The $\text{Bi}2$, $\text{Bi}3$, and Eu^{3+} emissions were observed besides the chip emission. CT, CRI and CIE were measured to be 4756 K , 65 , and $(0.3702, 0.2933)$. The CIE coordinate lies in the white range and it consists with the photo of the LED lamp (see the inset of Figure 16). This, as the proof of device, indicates that the phosphor can be used as a potential single-phased white emitting candidate for UV/NUV converted WLEDs.

4. CONCLUSIONS

In all, we have developed the single-phased X2-type $\text{Y}_2\text{SiO}_5:\text{Eu}^{3+},\text{Bi}^{3+}$ phosphor with the white light/tunable emissions by controlling the energy transfer via multi luminescent centers. It has weak absorption in visible range, and it can be excited by UV lights with the efficiency as high as 78%. For Bi^{3+} single doped Y_2SiO_5 , there are three emission peaks ($\text{Bi}1$, $\text{Bi}2$, and $\text{Bi}3$) at $\sim 360\text{--}408$ and $\sim 504 \text{ nm}$, respectively. The former two peaks are due to the substitutions of Bi^{3+} for $\text{Y}1$ and $\text{Y}2$ sites because of the higher covalency of the $\text{Y}(2)$ site. The latter at 504 nm should correlate to the Bi^{3+} ion which is bound to an oxygen vacancy, which is supported by the first principle calculations. Energy transfer happens from $\text{Bi}1$ to $\text{Bi}2$ and $\text{Bi}3$, and it is also from $\text{Bi}3$ to $\text{Bi}1$ and $\text{Bi}2$. But there is no backward energy transfer from $\text{Bi}2$ to $\text{Bi}3$. Tunable emission from blue to green can be made by proper selection of UV excitation wavelength in bismuth single doped Y_2SiO_5 . As Eu^{3+} is introduced into X2-type $\text{Y}_2\text{SiO}_5:\text{Bi}^{3+}$, white or tunable emissions can be realized by modulation of europium content or the excitation plans. In each UV excitation scheme, the energy transfer takes place from Bi^{3+} to Eu^{3+} via an electric dipole-dipole interaction, and the transfer efficiency can be

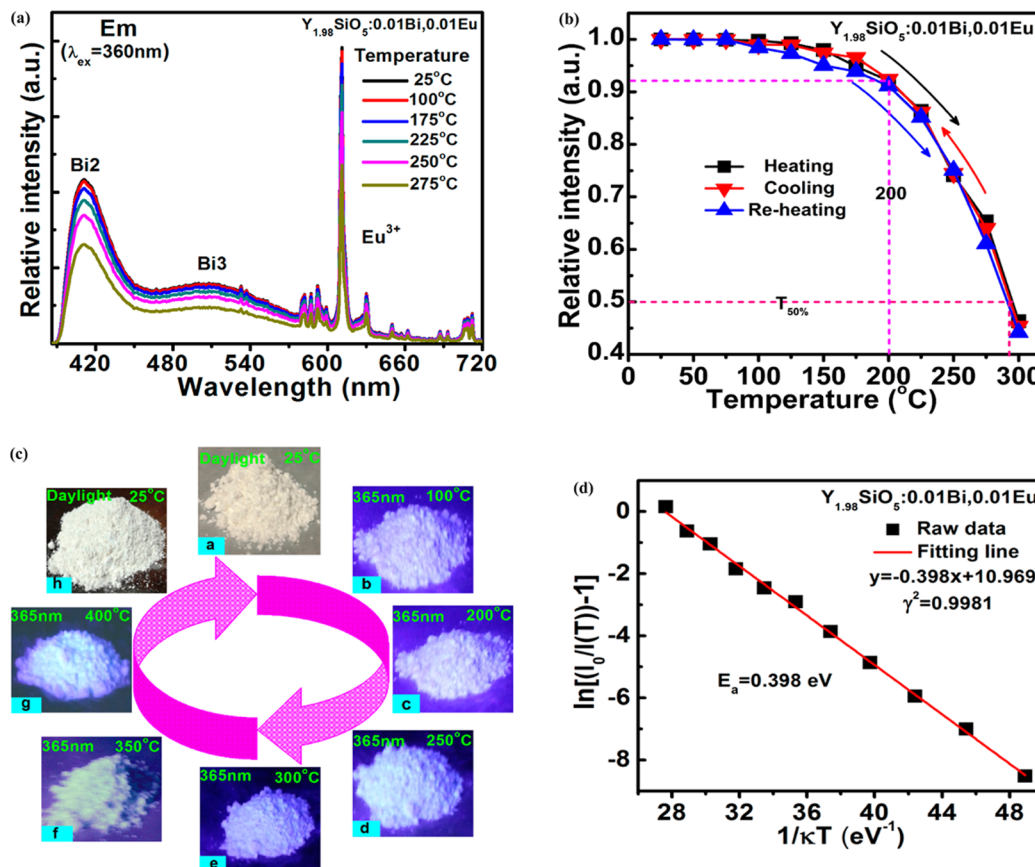


Figure 15. (a) Emission spectra ($\lambda_{\text{ex}} = 360 \text{ nm}$) of X2-type $\text{Y}_{1.98}\text{SiO}_5:0.01 \text{Bi}^{3+}, 0.01\text{Eu}^{3+}$ at temperature between 25 and 275 °C. (b) The temperature dependence of the integrated emission intensity of X2-type $\text{Y}_{1.98}\text{SiO}_5:0.01 \text{Bi}^{3+}, 0.01\text{Eu}^{3+}$ in three cycles of cooling and heating processes. (c) Sample photos under daylight and UV (~365 nm) lights at different temperatures. (d) Relationship of $\ln[(I_0/I(T)) - 1]$ versus $1/kT$ for the single-phased white light-emitting X2-type $\text{Y}_{1.98}\text{SiO}_5:0.01 \text{Bi}^{3+}, 0.01\text{Eu}^{3+}$ phosphor, and the fitted line (red) to eq 5

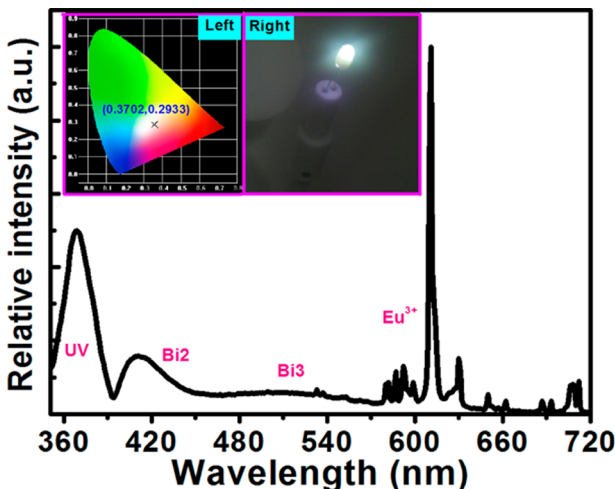


Figure 16. EL spectra of the WLED lamp fabricated by coating $\text{Y}_{1.98}\text{SiO}_5:0.01 \text{Bi}^{3+}, 0.01\text{Eu}^{3+}$ on an UV LED chip. Left and right insets are CIE chromaticity coordinates and image of the lamp driven by 20 mA current, respectively.

promoted by higher content of Eu³⁺, and the existence of Eu³⁺ does not block the transfer from Bi3 to Bi1 and Bi2. The optimized white emitting sample was found as X2-type $\text{Y}_{1.98}\text{SiO}_5:0.01 \text{Bi}^{3+}, 0.01\text{Eu}^{3+}$ and the yoyo experiments on cooling and heating cycles have confirmed the excellent resistance to thermal quenching and degradation. The thermal

quenching temperature $T_{50\%}$ is 293 °C with the activation energy 0.398 eV. These impressive results motivate us to evaluate the application of the phosphor in WLED. The WLED lamp has been developed by coating the phosphor onto an UV LED chip with color coordinate (0.3702, 0.2933) and color temperature 4756 K, and it proves the phosphor as a promising single-phased white light-emitting phosphor for UV/NUV converted WLEDs.

AUTHOR INFORMATION

Corresponding Author

*Tel: +86 20 87114204. Fax: +86 20 22236910. E-mail: pengmingying@scut.edu.cn.

Notes

The authors declare no competing financial interest.

ACKNOWLEDGMENTS

The authors would like to acknowledge financial support from the National Natural Science Foundation of China (Grant No. S1322208), Guangdong Natural Science Foundation for Distinguished Young Scholars (Grant No. S20120011380), the Department of Education of Guangdong Province (Grant No. 2013gjhz0001), and Fundamental Research Funds for the Central Universities (Grant No. 2013ZG004).

REFERENCES

- (1) Nakamura, S. *MRS Bull.* 1997, 22, 29–35.

- (2) Shang, M. M.; Li, G. G.; Kang, X. J.; Yang, D. M.; Geng, D. L.; Lin, J. *ACS Appl. Mater. Interfaces* **2011**, *3*, 2738–2746.
- (3) Xia, Z. G.; Liu, R. S. *J. Phys. Chem. C* **2012**, *116*, 15604–15609.
- (4) Zhang, X. G.; Zhou, L. Y.; Pang, Q.; Shi, J. X.; Gong, M. L. *J. Phys. Chem. C* **2014**, *118*, 7591–7598.
- (5) Huang, C. H.; Wu, P. J.; Lee, J. F.; Chen, T. M. *J. Mater. Chem.* **2011**, *21*, 10489–10495.
- (6) Shang, M. M.; Li, G. G.; Geng, D. L.; Yang, D. M.; Kang, X. J.; Zhang, Y.; Lian, H. Z.; Lin, J. *J. Phys. Chem. C* **2012**, *116*, 10222–10231.
- (7) Peng, M. Y.; Wondraczek, L. *Opt. Lett.* **2010**, *35*, 2544–2546.
- (8) Kang, F. W.; Yang, X. B.; Peng, M. Y.; Wondraczek, L.; Ma, Z. J.; Zhang, Q. Y.; Qiu, J. R. *J. Phys. Chem. C* **2014**, *118*, 7515–7522.
- (9) Yu, M.; Lin, J.; Fang, J. *Chem. Mater.* **2005**, *17*, 1783–1791.
- (10) Kang, F. W.; Peng, M. Y.; Zhang, Q. Y.; Qiu, J. Q. *Chem.—Eur. J.* **2014**, *20*, 11522–11530.
- (11) Peng, M. Y.; Wondraczek, L. *Opt. Lett.* **2009**, *34*, 2885–2887.
- (12) Peng, M. Y.; Wondraczek, L. *J. Am. Ceram. Soc.* **2010**, *93*, 1437–1442.
- (13) Guo, C. F.; Luan, L.; Xu, Y. X.; Gao, F.; Liang, L. F. *J. Electrochem. Soc.* **2008**, *155*, J310–J314.
- (14) Su, Y. G.; Li, L. P.; Li, G. S. *Chem. Mater.* **2008**, *20*, 6060–6067.
- (15) Su, Y. G.; Li, L. P.; Li, G. S. *J. Mater. Chem.* **2009**, *19*, 2316–2322.
- (16) Hu, Y. S.; Zhang, W. D.; Ye, H. Q.; Wang, D. H.; Zhang, S. S.; Huang, X. W. *J. Alloys Compd.* **2005**, *390*, 226–229.
- (17) Yan, S. X.; Zhang, J. H.; Zhang, X.; Lu, S. Z.; Ren, X. G.; Nie, Z. G.; Wang, X. *J. J. Phys. Chem. C* **2007**, *111*, 13256–13260.
- (18) Pust, P.; Weiler, V.; Hecht, C.; Tücks, A.; S.Wochnik, A.; Hen, A. K.; Wiechert, D.; Christina, S.; J. Schmidt, P.; Schnick, W. *Nat. Mater.* **2014**, *13*, 891–896.
- (19) Li, Y. Q.; Delsing, A. C. A; With, G. de.; Hintzen, H. T. *Chem. Mater.* **2005**, *17*, 3242–3248.
- (20) Oeckler, O.; A. Kechele, J.; Koss, H.; J. Schmidt, P.; Schnick, W. *Chem.—Eur. J.* **2009**, *15*, 5311–5319.
- (21) Xie, R. J.; Hirosaki, N. *Appl. Phys. Lett.* **2004**, *84*, 5404–5406.
- (22) Zhang, L. L.; Zhang, J. H.; Zhang, X.; Hao, Z. D.; Zhao, H. F.; Luo, Y. S. *ACS Appl. Mater. Interfaces* **2013**, *5*, 12839–12846.
- (23) Liu, X. L.; Liu, Y. X.; Yan, D. T.; Zhu, H. C.; Liu, C. G.; Xu, C. S.; Liu, Y. C.; Wang, X. *J. J. Mater. Chem.* **2012**, *22*, 16839–16843.
- (24) Lü, W.; Guo, N.; Jia, Y. C.; Zhao, Q.; Lv, W. Z.; Jiao, M. M.; Shao, B. Q.; You, H. P. *Inorg. Chem.* **2013**, *52*, 3007–3012.
- (25) Li, X. F.; Budai, J. D.; Liu, F.; Howe, J. Y.; Zhang, J. H.; Wang, X. J.; Gu, Z. J.; Sun, C. J.; Meltzer, R. S.; Pang, Z. W. *Light: Sci. Appl.* **2013**, *2* (e50), 1–8.
- (26) Lü, W.; Hao, Z. D.; Zhang, X.; Luo, Y. S.; Wang, X. J.; Zhang, J. H. *Inorg. Chem.* **2011**, *50*, 7846–7851.
- (27) Hirosaki, N.; Xie, R. J.; Kimoto, K. *Appl. Phys. Lett.* **2005**, *86*, No. 211905.
- (28) Xie, R. J.; Hirosaki, N.; Li, Y. Q.; Takeda, T. *Materials* **2010**, *3*, 3777–3793.
- (29) Kim, J. S.; Jeon, P. E.; Park, Y. H.; Choi, J. C.; Park, H. L. *Appl. Phys. Lett.* **2004**, *85*, 3696–3698.
- (30) Chen, D. Q.; Wang, Y. S.; Zheng, K. L.; Guo, T. L.; Yu, Y. L.; Huang, P. *Appl. Phys. Lett.* **2007**, *91*, No. 251903.
- (31) Zhuang, Y. X.; Ueda, J. P.; Tanabe, S. *Opt. Mater. Express* **2012**, *2*, 1378–1383.
- (32) Shi, L.; Seo, H. J. *Opt. Express* **2011**, *19*, 7147–7152.
- (33) Geng, D. L.; Shang, M. M.; Zhang, Y.; Cheng, Z. Y.; Lin, J. *Eur. J. Inorg. Chem.* **2013**, 2947–2953.
- (34) Ci, Z. P.; Sun, Q. S.; Sun, M. X.; Jiang, X. J.; Qin, S. C.; Wang, Y. H. *J. Mater. Chem. C* **2014**, *2*, 5850–5856.
- (35) Liu, Y. F.; Zhang, X.; Hao, Z. D.; Wang, X. J.; Zhang, J. H. *Chem. Commun.* **2011**, *47*, 10677–10679.
- (36) Guo, L. N.; Wang, Y. H.; Zhang, J.; Dong, P. Y. *J. Electrochem. Soc.* **2011**, *158*, J225–J229.
- (37) Shang, M. M.; Li, C. X.; Lin, J. *Chem. Soc. Rev.* **2014**, *43*, 1372–1386.
- (38) Dorman, J. A.; Choi, J. H.; Kuzmanich, G.; Chang, J. P. *J. Phys. Chem. C* **2012**, *116*, 12854–12860.
- (39) Wang, W. N.; Ogi, T.; Kaihatsu, Y.; Iskandar, F.; Okuyama, K. *J. Mater. Chem.* **2011**, *21*, 5183–5189.
- (40) Deka, C.; Chai, B. H. T.; Shimony, Y.; Zhang, X. X.; Munin, E.; Bass, M. *Appl. Phys. Lett.* **1992**, *61*, 2141–2143.
- (41) Shin, S. H.; Jeon, D. Y.; Suh, K. S. *Jpn. J. Appl. Phys.* **2001**, *40*, 4715–4719.
- (42) Saha, S.; Chowdhury, P. S.; Patra, A. *J. Phys. Chem. B* **2005**, *109*, 2699–2702.
- (43) Liu, Y.; Xu, C. N.; Nonaka, K.; Tateyama, H. *J. Mater. Sci.* **2011**, *36*, 4361–4364.
- (44) Yin, M.; Duan, C.; Zhang, W.; Lou, L.; Xia, S.; Krupa, J. C. *J. Appl. Phys.* **1999**, *86*, 3751–3757.
- (45) Kang, Y. C.; Lenggoro, I. W.; Okuyama, K.; Park, S. B. *J. Electrochem. Soc.* **1999**, *146*, 1227–1230.
- (46) Marsh, P. J.; Silver, J.; Vecht, A.; Newport, A. *J. Lumin.* **2002**, *97*, 229–236.
- (47) Lin, J.; Su, Q.; Wang, S.; Zhang, H. *J. Mater. Chem.* **1996**, *6*, 265–269.
- (48) Wen, J.; Duan, C. K.; Ning, L. X.; Huang, Y. C.; Zhan, S. B.; Zhang, J.; Yin, M. *J. Phys. Chem. A* **2014**, *118*, 4988–4994.
- (49) Kang, F. W.; Peng, M. Y. *Dalton Trans.* **2014**, *43*, 277–284.
- (50) Kang, F. W.; Peng, M. Y.; Xu, S. H.; Ma, Z. J.; Dong, G. P.; Qiu, J. R. *Eur. J. Inorg. Chem.* **2014**, 1373–1380.
- (51) Wang, W. X.; Yang, P. P.; Cheng, Z. Y.; Hou, Z. Y.; Li, C. X.; Lin, J. *ACS Appl. Mater. Interfaces* **2011**, *3*, 3921–3928.
- (52) Jia, P. Y.; Liu, X. M.; Li, G. Z.; Yu, M.; Fang, J.; Lin, J. *Nanotechnology* **2006**, *17*, 734–742.
- (53) Li, P. F.; Peng, M. Y.; Yin, X. W.; Ma, Z. J.; Dong, G. P.; Zhang, Q. Y.; Qiu, J. R. *Opt. Express* **2013**, *21*, 18943–18948.
- (54) Kang, F. W.; Zhang, Y.; Wondraczek, L.; Zhu, J. Q.; Yang, X. B.; Peng, M. Y. *J. Mater. Chem. C* **2014**, *2*, 9850–9857.
- (55) Lv, W. Z.; Jia, Y. C.; Zhao, Q.; Jiao, M. M.; Shao, B. Q.; Lü, W.; You, H. P. *Adv. Optical Mater.* **2014**, *2*, 183–188.
- (56) Xie, R. J.; Hirosaki, N.; Suehiro, T.; Xu, F. F.; Mitomo, M. *Chem. Mater.* **2006**, *18*, 5578–5583.
- (57) Wang, X. C.; Seto, T.; Zhao, Z. Y.; Li, Y. Y.; Wu, Q. S.; Li, H.; Wang, Y. H. *J. Mater. Chem. C* **2014**, *2*, 4476–4481.